Breaking of symmetry in microfluidic propulsion driven by artificial cilia

Khaderi, S. N.; Baltussen, M. G. H. M.; Anderson, P. D.; den Toonder, J.M.J.; Onck, P. R.

Published in:
Physical Review E

DOI:
10.1103/PhysRevE.82.027302

Publication date:
2010

Breaking of symmetry in microfluidic propulsion driven by artificial cilia

S. N. Khaderi,[1] M. G. H. M. Baltussen,[2] P. D. Anderson,[2] J. M. J. den Toonder,[2] and P. R. Onck[1,*]
[1]*Zernike Institute for Advanced Materials, University of Groningen, Groningen, The Netherlands*
[2]*Eindhoven University of Technology, Eindhoven, The Netherlands*
(Received 25 May 2010; published 25 August 2010)

In this Brief Report we investigate biomimetic fluid propulsion due to an array of periodically beating artificial cilia. A generic model system is defined in which the effects of inertial fluid forces and the spatial, temporal, and orientational asymmetries of the ciliary motion can be individually controlled. We demonstrate that the so-far unexplored orientational asymmetry plays an important role in generating flow and that the flow increases sharply with Reynolds number and eventually becomes unidirectional. We introduce the concept of configurational symmetry that unifies the spatial, temporal, and orientational symmetries. The breaking of configurational symmetry leads to fluid propulsion in microfluidic channels.

DOI: 10.1103/PhysRevE.82.027302 PACS number(s): 47.61.−k

One of the principal challenges in lab-on-a-chip applications is to propel the fluids in microchannels [1]. To propel fluids at these small length scales, nature utilizes cilia and flagella attached to the surface of organisms to actuate the fluid locally so as to have a net fluid propulsion. A consequence of the small length scales is that viscous forces dominate over inertial forces, which dictates that the actuators have to move periodically in time but in a spatially asymmetric manner. This condition is satisfied in the case of cilia by the distinct effective and recovery stroke during each cycle of their motion [2].

Many examples have appeared in the recent literature of artificial cilia that mimic the natural ciliary motion through different physical actuation forces, imposed by electric fields, magnetic fields, or through base excitation [3–13]. In some cases the physical actuation forces get sufficiently large, so that also the effect of inertia comes into play [4,14]. As a result, the breaking of temporal asymmetry can also contribute to propulsion, in addition to the breaking of spatial asymmetry as required at low Reynolds numbers. In general, there are three fundamental mechanisms that are active in artificial cilia-driven fluid flow: (i) spatially asymmetric motion, (ii) temporally asymmetric motion, and (iii) orientationally asymmetric motion. The first is the only mechanism that is effective at low Reynolds numbers. Nature effectively makes use of this at small length scales (e.g., cilia). In addition to spatial asymmetry, temporal asymmetry can enhance flow when inertial forces are no longer negligible (e.g., the locomotion of scallops is entirely based on spatially symmetric motion with temporal asymmetry). In human swimming both spatial and temporal asymmetries are employed. The third mechanism has not been carefully explored until now and is related to the asymmetry of the actuator motion relative to the channel direction. However, due to the intricate interplay of actuation forces (e.g., electric and magnetic), elastic forces, fluid inertia, and drag forces, the individual contributions of the three fundamental mechanisms to the generated flow remain unknown.

To understand how the fluid flow depends individually on these mechanisms, we analyze a model system in which the relative contribution of the spatial, temporal, and orientational asymmetries can be studied as a function of fluid inertia. We show that the inertial forces in the fluid can be usefully exploited to enhance the flow when compared to the flow in the Stokes regime. Moreover, by utilizing the inertial forces the flow can be made unidirectional, even though the ciliary motion is cyclic. Interestingly, also natural cilia are able to generate a unidirectional flow, but utilize metachrony to achieve this [15]. In the absence of any spatial and temporal asymmetries, the orientational symmetry can be broken which leads to flow rates that are comparable to typical spatially asymmetric rates in the Stokes regime. Finally, we unify the asymmetries studied in this analysis and introduce the general concept of configurational symmetry, the breaking of which causes flow.

We study a two-dimensional model system consisting of an infinitely long array of synchronously beating cilia with an interciliary spacing W, placed in a channel of height H. To perform the simulations, we choose a unit cell of width $W=2L$ and height $H=2L$, whose top and bottom are no-slip boundaries and the left and right boundaries are periodic (see Fig. 1). We kinematically prescribe the motion of the cilium such that its tip moves in an elliptical orbit around $(x,y)=(0,0)$, at an angular velocity of $\omega_e=2\pi/T_e$ for the effective stroke and $\omega_r=2\pi/T_r$ for the recovery stroke, resulting in a total cycle time $t_{\text{cycle}}=(T_e+T_r)/2$. Here, $T_e/2$ and $T_r/2$ are the times taken to complete the effective and recovery strokes, respectively. The lengths of the principal elliptical axes are $2a$ and $2b$, oriented at an angle θ to the channel direction. The remaining portion of the cilium is kinemati-

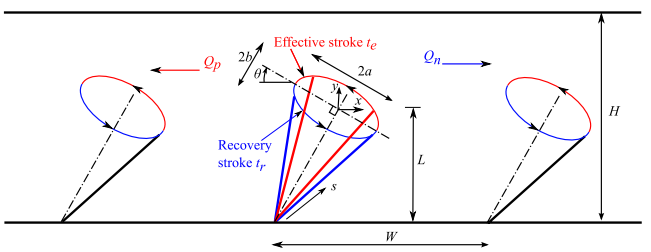

FIG. 1. (Color online) Schematic picture of the model problem showing the parameters involved.

*Corresponding author. p.r.onck@rug.nl

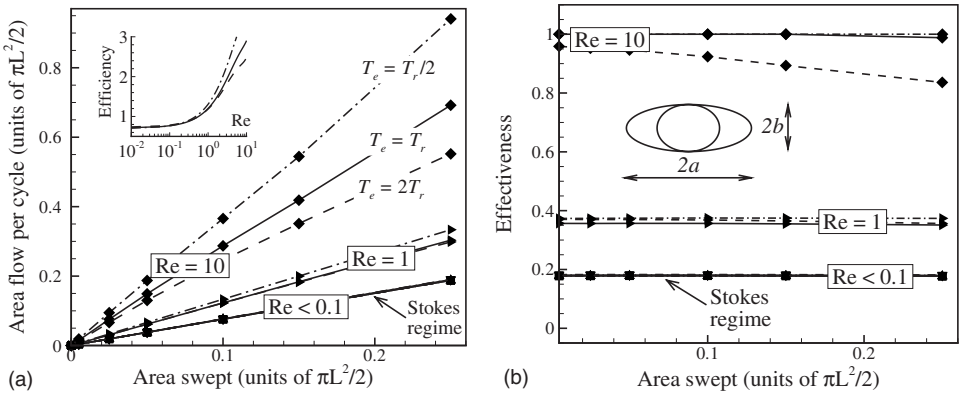

FIG. 2. (a) Area flow per cycle as a function of the area swept (θ=0°) for different Reynolds numbers. Also plotted are the cases in which the velocity during the effective stroke is different from that of the recovery stroke. The inset shows the efficiency of fluid flow as a function of the Reynolds number. (b) Effectiveness of fluid flow $[(Q_p-Q_n)/(Q_p+Q_n)]$ as a function of the area swept for different Reynolds numbers and T_e/T_r values.

cally prescribed to remain straight, with the lower end of the film fixed at $(-L\tan\theta,-L)$. The angle θ is zero when the principal elliptical axis $2a$ is parallel to the channel axis and is positive in the clockwise direction; the orientation shown in Fig. 1 corresponds to $\theta>0$. Note that the center of the elliptical orbit is fixed for all cases analyzed (i.e., L remains constant), while θ can be independently varied. The inertia in the fluid is independently controlled by changing the Reynolds number ($\mathrm{Re}=\rho L^2/\mu t_{\mathrm{cycle}}$) through the fluid density ρ, while the fluid viscosity μ is maintained constant. The temporal asymmetry is controlled by changing T_e/T_r, while the total cycle time $(T_e+T_r)/2$ is maintained constant. It is to be noted that when $a=0$ or $b=0$ no spatial asymmetry exists, when $T_e=T_r$ no temporal asymmetry exists, and when $\theta=0$ no orientational asymmetry exists. All three asymmetries can be independently controlled.

The defined problem is solved using the finite element method in which the fluid is assumed to be an incompressible Newtonian liquid. The fluid-structure interaction is performed using the fictitious domain method in which the fluid and the solid (cilia) velocities are coupled through Lagrange multipliers [10,16]. The instantaneous flux is obtained by integrating the horizontal velocity over the channel height, while the net amount of fluid propelled per cycle (termed "area flow") is calculated by integrating the instantaneous flux over the cycle time. The fluid is initially at rest and it takes some time for the system to reach a steady state, especially at large Reynolds numbers (for the results presented, the system reaches a steady state within 4 cycles). The outcome of the analysis is quantified in terms of three parameters after a steady state has been reached: the area flow, the efficiency, and the effectiveness of fluid transport. The latter two are detailed in the following. The cilium pushes the fluid forward during the effective stroke, creating a "positive area flow" Q_p in the direction of the effective stroke (i.e., to the left in Fig. 1) and pushes the fluid back during the recovery stroke creating a "negative area flow" Q_n. Under suitable conditions, the positive flow is larger than the negative flow, generating a positive area flow per cycle (Q_p-Q_n). The effectiveness, defined as $(Q_p-Q_n)/(Q_p+Q_n)$, indicates which part of the totally displaced fluid is effectively converted into a net flow. An effectiveness of unity represents a unidirectional flow. To investigate how efficiently the swept area (area of the ellipse) is converted to fluid flow, we define the efficiency as the area flow per unit area swept.

We first study the dependence of the area flow on the area swept, Reynolds number, and temporal asymmetry T_r/T_e for a fixed orientation θ=0 in Fig. 2. The swept area is changed by fixing b and changing a. Both the area flow and the swept area are normalized with $(\pi L^2/2)$. It can be seen that for all values of Reynolds number the area flow scales linearly with the swept area [Fig. 2(a), as also observed in [10] for the Stokes regime]. It can be seen from the inset of Fig. 2(a) that for $\mathrm{Re}<0.1$ (Stokes limit) the efficiency (i.e., the area flow per unit area swept) remains constant, while for $\mathrm{Re}>0.1$ the efficiency increases sharply with an increase in Reynolds number. Moreover, at high Reynolds numbers the flow generated increases when the effective stroke is faster than the recovery stroke $(T_e<T_r)$, while it decreases when the opposite is true $(T_e>T_r)$. Figure 2(b) shows the effectiveness as a function of area swept. The effectiveness is low when a large volume of fluid is shifted back and forth with only a modest net effect. This is the case in the Stokes regime. However, with increasing Reynolds number the effectiveness increases, reaching a purely unidirectional flow at $\mathrm{Re}\approx 10$ and for relatively fast effective strokes. As b is kept constant and a is increased, the velocity of the cilium is enhanced because the cycle time is fixed. Hence, as the swept area is increased, the instantaneous flux also increases due to the larger velocity during the effective as well as the recovery stroke. This results in the effectiveness of fluid actuation to be unchanged [Fig. 2(b)], but causes an increase in the net area flow due to the enhanced fluid velocity [Fig. 2(a)].

To analyze how the fluid is pumped through each cycle we plot the trajectory of fluid particles for 2 cycles in Fig. 3. We compare the results in the Stokes limit [low Re, Fig. 3(a)] with those at large Re [Re=10, Fig. 3(b)]. Animations of these simulations including the fluid velocity fields are provided as supplementary material [17]. The fluid particles are represented by dots forming initially a straight line in instance 1. Instances 3 and 5 refer to the end of the first and the second cycles, respectively, and instances 2 and 4 refer to

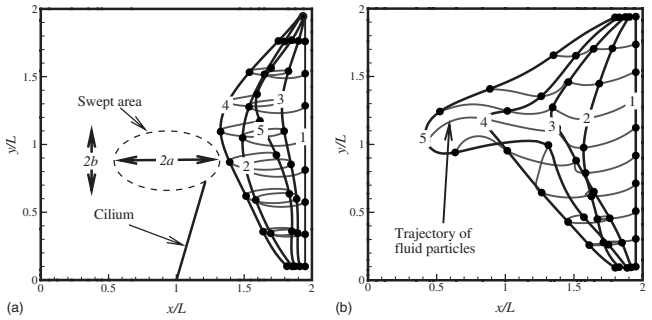

FIG. 3. Trajectory of particles over 2 cycles for $T_e=T_r$, $\theta=0$, $a=0.3L$, and $b=0.25L$. (a) Stokes regime (Re<0.1); (b) Re$=10$. The fluid particles initially form a straight line indicated by line 1 and move to positions along curves 2–5 in 2 cycles of cilia motion. Animations of these cases including the fluid velocity fields are added as supplementary material [17].

the end of the effective stroke of the first and second cycles. In the Stokes limit [i.e., low Re; see Fig. 3(a)], the dissipative viscous forces are larger than the inertial forces. As a consequence, the energy gained by the fluid due to the actuation of the cilium will be instantaneously dissipated, so that the momentum imparted by the cilium will be efficiently (instantaneously) transmitted to the surrounding fluid without delay. The fluid particles which initially form a straight line (instance 1) move due to the velocity imposed by the film during the effective stroke. The fluid particles stop and reverse their direction of motion once the film begins the recovery stroke (at instances 2 and 4) leading to backflow during recovery (ending at instances 3 and 5). Due to the spatial asymmetry in the deformation of the film, we observe a net displacement of fluid particles over each cycle. As the fluid particles move back and forth during the cycle, the flow exhibits a fluctuating behavior, leading to a low effectiveness of fluid propulsion [see Fig. 2(b)]. The response of the system does not change when the effective and recovery strokes are performed at different rates.

When the Reynolds number is high [Fig. 3(b)], the dissipative forces are low compared to the inertial forces. Hence, the inertial momentum or energy gained by the fluid during the effective stroke is not dissipated instantaneously, but persists during recovery, which causes a flux in the direction of the effective stroke even during the recovery stroke (see instances 2-3 and 4-5). This effect becomes more prominent as the Reynolds number is increased, leading to a large net fluid flow [Fig. 2(a)], high efficiency [inset of Fig. 2(a)], and a higher effectiveness [Fig. 2(b)]. The flow becomes fully unidirectional for $T_e=T_r$ when Re≥ 10. Note that the particles close to the bottom boundary still fluctuate even at high Re. This is due to the fact that in this region the momentum is not transmitted through viscous forces, but due to the pressure gradient between adjacent cilia. This mode of momentum transfer is equally efficient at low as well as high Reynolds numbers (see Fig. 3).

From the results presented so far, the effects of spatial and temporal asymmetries are independently studied, in the absence of orientational asymmetry ($\theta=0$). To analyze the effect of orientational asymmetry we analyze the flow as a function of the orientation θ in the absence of spatial asymmetry ($a=0.25L$ and $b=0$) in Fig. 4. The temporal asymmetry is varied from $T_r=T_e$ (no asymmetry) to $T_r=3T_e$ and the direction of ciliary motion θ from $-60°$ to $60°$ (see Fig. 1) for different Reynolds numbers. The area flow is normalized with $\pi L^2/2\cos^2\theta$. When the motion of the cilium exhibits no temporal asymmetry, we do not observe flow in the Stokes regime (Re<0.1), for all orientations θ. Now, as we increase the Reynolds number (still $T_r=T_e$), a fluid flow is observed whose direction depends on the orientation θ, reaching a maximum at $\theta=\pm 45°$; see the dotted lines in Fig. 4. The results are point symmetric in (0,0) due to the absence of any spatial and temporal asymmetries. The flow generated is therefore entirely due to the breaking of orientational symmetry. When $\theta=-45°$ we obtain a maximal positive flow (i.e., flow in the direction of the effective stroke; see Fig. 1) and when the film moves in the direction $\theta=45°$ we observe a negative flow. When we allow for temporal asymmetry (i.e., $T_e<T_r$), the flow is enhanced in the direction of the effective stroke (positive flow), the extent of which is larger for $\theta<0$ compared to $\theta>0$.

Consider the case when no temporal asymmetry exists ($T_r=T_e$), i.e., the dotted lines in Fig. 4, for $\theta=-45°$. An animation of this case is added as supplementary material [17]. During the effective stoke, the cilium imparts momentum to the fluid as it moves toward the bottom boundary and away from the moving fluid, allowing the fluid to pass without much obstruction in the direction of the effective stroke. When the cilium performs a recovery stroke, it again imparts momentum to the fluid, but now the cilium moves away from the bottom boundary thereby obstructing the flow during recovery. During the cycle, we thus have a larger flow during the effective stroke than during the recovery stroke, resulting in a net positive fluid flow in the effective direction. It is interesting to note that the observed net flow originates solely from the orientational asymmetry, causing an easy passage of fluid during the effective stroke while obstructing the flow during the recovery. Since there is no spatial or

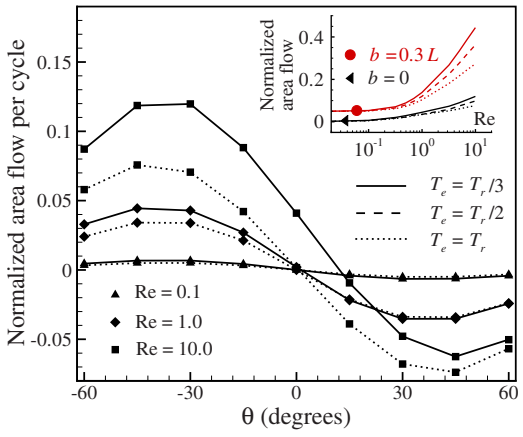

FIG. 4. (Color online) Area flow per cycle normalized with $\pi L^2/2\cos^2\theta$ as a function of orientation θ for different Reynolds numbers and temporal asymmetries. The inset shows the normalized area flow per cycle as a function of Reynolds number (Re) for $\theta=-45°$ for different temporal and spatial asymmetries. In all the simulations a is taken to be equal to $0.25L$. An animation is added as supplementary material for $\theta=-45°$ and $T_e=T_r$ [17].

temporal asymmetry, the problem is perfectly symmetric with respect to $\theta=0$, resulting in equal-sized but opposite flows for $\theta=45°$. When the fluid is pushed at a higher rate during the effective stroke, i.e., $T_e<T_r$ (solid lines in Fig. 4), for $\theta<0$ the motion of the film allows an easy passage of the high-momentum fluid during the effective stroke, while obstructing the low-momentum fluid during recovery. For $\theta>0$, the film motion obstructs the high-energy fluid during the effective stroke and allows easy passage of low-energy fluid during recovery, resulting in a much smaller enhancement of positive flow than for $\theta<0$. In the inset of Fig. 4 we analyze flow as a function of Reynolds number for $\theta=-45°$, in the presence ($b=0.3L$) and absence ($b=0$) of spatial asymmetry. It can be observed that fluid propulsion can be generated when no temporal and spatial asymmetries exist, provided the fluid inertia is non-negligible (lowest curve). The flow can be increased by including temporal asymmetry (i.e., faster effective than recovery stroke). By adding spatial asymmetry, the effect of orientational and temporal asymmetries can be drastically enhanced, leading to a synergistic combination of all three asymmetries.

The three independent symmetries studied in this Brief Report, i.e., spatial, temporal, and orientational symmetries, can be generalized into the concept of configurational symmetry. We define a ciliary configuration at any time t by the position of material points $s(x,y)$ of the cilium and their instantaneous velocities $(\dot{x},\dot{y})$. We define the system to be configurationally symmetric when every configuration (at time t) can find its mirror image after half a cycle (at time $t+t_{\text{cycle}}/2$), with the symmetry plane being perpendicular to the channel (see Fig. 5). A net flow will occur in the absence of configurational symmetry. This symmetry can be broken by spatial, temporal, or orientational asymmetry.

It is interesting to note that even a nonreciprocal motion can be configurationally symmetric. For instance, an actuator beating like a flagellum and aligned normal to the channel axis will find its mirror image after half a cycle and therefore will not generate a net flow. Such an actuator needs to be nonperpendicular to the channel direction in order to break the orientational symmetry and to generate a flow, as has been shown in [18]. Examples in the literature where the configurational symmetry is broken through spatial asymmetry leading to fluid flow can be found in [6,8–10], employing actuation forces that are generated by magnetic fields [9,10], internal molecular motors [8], and light [6]. In the case of electrostatic artificial cilia [4], the fluid flow was achieved by breaking both temporal and orientational symmetries. On the other hand, a nice example of configurationally symmetric cilia is given in [5], where it is shown that a configurationally symmetric motion of cilia cannot generate a fluid flow in the direction of the channel. Thus, the definition of configurational symmetry can be a valuable fundamental concept in understanding existing (and designing new) physical actuation mechanisms for microfluidic propulsion. Moreover, it opens the opportunity of deriving analytical expressions that relate flow to quantitative measures of configurational asymmetry.

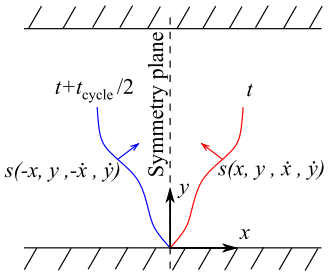

FIG. 5. (Color online) Definition of configurational symmetry: every ciliary configuration [i.e., the current position of all material points $s(x,y)$ and their velocities $(\dot{x},\dot{y})$] at time t can find its mirror image after half a cycle with the symmetry plane being perpendicular to the channel.

This work is a part of the 6th Framework European project "Artic," under Contract No. STRP 033274.

[1] D. J. Laser and J. G. Santiago, J. Micromech. Microeng. **14**, R35 (2004).
[2] C. Brennen and H. Winet, Annu. Rev. Fluid Mech. **9**, 339 (1977).
[3] B. A. Evans, A. R. Shields, R. L. Carroll, S. Washburn, M. R. Falvo, and R. Superfine, Nano Lett. **7**, 1428 (2007).
[4] J. den Toonder *et al.*, Lab Chip **8**, 533 (2008).
[5] K. Oh, J.-H. Chung, S. Devasia, and J. J. Riley, Lab Chip **9**, 1561 (2009).
[6] C. L. van Oosten, C. W. M. Bastiaansen, and D. J. Broer, Nature Mater. **8**, 677 (2009).
[7] F. Fahrni, M. W. J. Prins, and L. J. van IJzendoorn, Lab Chip **9**, 3413 (2009).
[8] Y. W. Kim and R. R. Netz, Phys. Rev. Lett. **96**, 158101 (2006).
[9] E. M. Gauger, M. T. Downton, and H. Stark, Eur. Phys. J. E **28**, 231 (2009).
[10] S. N. Khaderi, M. G. H. M. Baltussen, P. D. Anderson, D. Ioan, J. M. J. den Toonder, and P. R. Onck, Phys. Rev. E **79**, 046304 (2009).
[11] A. Alexeev, J. M. Yeomans, and A. C. Balazs, Langmuir **24**, 12102 (2008).
[12] M. T. Downton and H. Stark, EPL **85**, 44002 (2009).
[13] R. Ghosh, G. A. Buxton, O. B. Usta, A. C. Balazs, and A. Alexeev, Langmuir **26**, 2963 (2010).
[14] M. G. H. M. Baltussen, P. D. Anderson, F. M. Bos, and J. M. J. den Toonder, Lab Chip **9**, 2326 (2009).
[15] P. Satir and M. A. Sleigh, Annu. Rev. Physiol. **52**, 137 (1990).
[16] R. van Loon, P. Anderson, F. van de Vosse, and S. Sherwin, Comput. Struct. **85**, 833 (2007).
[17] See supplementary material at http://link.aps.org/supplemental/10.1103/PhysRevE.82.027302 for animations of simulations.
[18] N. Darnton, L. Turner, K. Breuer, and H. C. Berg, Biophys. J. **86**, 1863 (2004).